Available online at www.eccomasproceedia.org
Eccomas Proceedia COMPDYN (2023) 3077-3090

ECCOMAS
Proceedia

COMPDYN 2023
9th ECCOMAS Thematic Conference on
Computational Methods in Structural Dynamics and Earthquake Engineering
M. Papadrakakis, M. Fragiadakis (eds.)
Athens, Greece, 12-14 June 2023

# EXPERIMENTAL AND FINITE ELEMENT ANALYSIS OF THE CYCLIC BEHAVIOUR OF LINEAR DISSIPATIVE DEVICES

**Salvatore Pagnotta, Muhammad Ahmed and Piero Colajanni**

Department of Engineering, University of Palermo,
Viale delle Scienze, Ed. 8, 90128, Palermo, Italy.
email: {salvatore.pagnotta, muhammad.ahmed, piero.colajanni}@unipa.it

## Abstract

In the past years, low-damage design of structures is becoming an efficient approach by engineers and researchers in order to mitigate the structural damage to buildings during a seismic event. To this aim, one of the most popular strategies is to endow framed structures with either viscous, hysteretic metallic, or viscoelastic devices. As an alternative to these systems, friction devices have been also studied, proving to be an effective solution. Steel braces endowed with linear dissipative devices based on friction can be used effectively both in the case of new and existing structures. Studies conducted on these devices stressed that their behaviour is mainly influenced by type of friction materials, loss of bolt preload and effect of disc springs.
An experimental campaign has been performed at the Materials and Structures Laboratory of the University of Palermo on linear dissipative devices with different types of friction materials i.e., steel, thermal sprayed aluminium, and brass, to check their effectiveness. Finite element analysis using ABAQUS has been done to design, check the functionality, and get insight into the experimental results of the linear dissipative devices. An investigation has been done on the effectiveness of disc springs to limit the bolt preload variation in the device and the effect of thicknesses of plates on the functionality of linear friction dissipative device. The results showed that thermal sprayed aluminium, coupled with structural steel, is a good friction material as it provides stable hysteresis loops and high friction coefficient as compared to brass, and appropriately designed disc springs are able to limit bolt preload variation.
The experimental results showed that the thermal sprayed aluminium provides a friction coefficient between 0.57 and 0.6 without significant variation even for a large number of cycles, while for the brass the friction coefficient at the beginning of the test was 0.25 and then it increased to 0.45 at the end of test, exhibiting large variation due to stick and slip phenomenon. The FEM analysis proved that the disc springs are able to minimize the variation of the contact pressure due to the Poisson effect and proper thickness of friction plates are important for the performance of friction device.

**Keywords:** Friction, Energy dissipation, Pre-load, Cyclic loading.

ISSN:2623-3347 
Peer-review under responsibility of the organizing committee of COMPDYN 2023.
doi: 10.7712/120123.10624.21461

## 1 INTRODUCTION

During the last decades, an increase in seismic events urges a need to ensure an effective dissipative global behaviour for structures in order to prevent them from collapsing and to mitigate the chances of loss of human lives. Design strategies for seismic-resistant buildings and seismic rehabilitation of existing buildings have become one of the most important topics among researchers. Depending on the type of structure different retrofitting techniques, either through a global modification of structural seismic behavior [1], or through simple local interventions [2], were proposed.

The use of dissipative connection in the designing of seismic resistant low damage steel frame was investigated by several authors [5]-[9], while more recently a friction device for beam to column connection was proposed for reinforced concrete frames with Hybrid Steel Truss Concrete Beams (HSTCB)s by [10]-[13].

Detailed and well-designed friction devices are an efficient solution to dissipate seismic energy and provide stable hysteresis behaviour using different friction materials [14]. Over the last few years friction devices have been also studied as an alternative to viscous, hysteretic metallic, viscoelastic etc. proving to be an effective solution.

Retrofitting of either steel or reinforced concrete frames by bracing equipped with dissipative devices has been recognized as one of the most performing and economic procedure. The use of friction-based dissipative devices started in the eighties of the last century [15] and recently has gained more popularity. Their use is still growing in the seismic active regions because of the economic and safety aspect [16].

In order to ensure a highly dissipative behaviour of linear friction dissipative device, two aspects are mainly investigated: variation of friction coefficient and contact pressure during the operational condition, that provide the sliding force of the device. In general, the main phenomena that can occur on the surfaces on which friction forces are generated are the increase in the roughness of surfaces with a smooth finish, which leads to an increase in the coefficient of friction and flattening of the roughness of surfaces with a rough finish, which leads to a decrease in the coefficient of friction. It is evident how such phenomena can make the behaviour of dissipative friction connections uncontrollable, that's why the choice of the friction material to be adopted must fall on those materials whose properties do not change significantly during the sliding of the surfaces.

As regards the second aspect, i.e., contact pressure, its value in operation is affected both by the application procedure of the bolt preload and by long-term phenomena. In fact, with the common techniques used to preload bolts (for example the use of a torque wrench), it is extremely complex to precisely control the level of force applied.

When friction devices are utilized as a dissipative source in beam-to-column friction joints, many aspects are investigated, such as stiffness and strength of the connection, amplitude, stability and symmetry of hysteresis cycles, recentering behaviour and influence on the global response of the structure.

Regarding the behaviour of linear dissipative devices, [17] investigated the cyclic response of linear dissipative devices using different friction materials by performing cyclic tests under the displacement control method, analyzing the variation of friction coefficient. They found that thermal sprayed aluminium on the steel interface has a consistent cyclic response and less variation of friction coefficient, remaining nearly constant with just 3-5% variation between the start and end of the test. It was also found that it has a high value of friction coefficient (0.5-0.6) as compared to the steel-steel, which ranges between 0.18 and 0.35 during the test, and brass on steel (ranging from 0.1 to 0.25).

To understand the preload behaviour, [18] investigated the actual preload levels applied on a series of bolts, applied by reading the tightening torque provided by a torque wrench. The force actually applied was measured by means of a load cell placed between the bolt head and the steel plate in which the bolt was inserted. They found that the dispersion of the data was significant, having a preload force with 95% fractile equal to 112.3% of the nominal value, while with 5% fractile equal to 96.4%. It is therefore evident that how such uncertainty of the preload force applied to the bolts directly influences the uncertainty of the sliding load of the friction device.

In addition to this uncertainty, the value of the prestressing load in operation is affected by the long-term preload loss that occurs in the bolts due to creep phenomena and by the crushing of the asperities on the surfaces in contact between the nut, pin and washer. In order to minimize these effects, several authors [19] proposed to keep the preload in the bolts between 30% and 60% of the maximum applicable according to Eurocode 3.

In addition to reducing the maximum preload applied to the bolts, the main solution adopted to limit the variations in preload is the use of cup springs or conical washers. These are truncated cone-shaped washers that are arranged below the nuts and bolt heads in different configurations based on the required force-lowering behaviour.

Another aspect to take into account in the design of structures equipped with friction devices is the dependence of the mechanical behaviour of these elements on the speed of application of the load. In fact, it has been seen that as the speed of displacement varies, these systems offer a mechanical response (in terms of force/sliding moment) which is greater than that obtained with quasi-static type tests [20][21]. This difference depends not only on the imposed movement speed, but also on the type of the used friction material.

In [22] experimental analysis was done on both friction-based linear dissipative devices and friction-based beam-to-column joints using thermal sprayed aluminium as a friction material. The material selection was done on the basis of its performance reported in the literature [8][17][19][23][24]. The results showed that in the friction-based beam-to-column joint hysteresis cycles were unexpectedly not symmetrical, so it urges a need to get more insight into the friction-based dissipative device behaviour, in order to detect the source of this unexpected behaviour.

In this paper, to develop the technical knowledge regarding the role of friction devices for the strengthening of frames and to check the functionality of a linear dissipative device, two approaches were adopted i.e., FEM and experimental analysis. To analyze the friction properties of different materials to be used in a linear dissipative device, a linear friction dissipative device was tested using the cyclic loading protocol as suggested in code [25].

In the experimental campaign, on the basis of the previously mentioned results in the literature, two materials were investigated, namely thermal-sprayed aluminium and brass, both coupled with structural steel. The variation of bolt preload during the test was evaluated using load cells, while the evaluation of the friction coefficient was done by a correlation between sliding force and the actual instant value of preload acting on the bolts.

FEM analysis has been done to further check the functionality and to deeply analyze the behaviour of aluminium plates with different thicknesses, and the role of disc springs. In the FEM analysis, the same testing protocols and properties were taken into consideration as of the experimental test but with different thicknesses of thermal sprayed aluminium plates.

## 2 DESIGN OF LINEAR DISSIPATIVE DEVICES

The reference test specimen was similar to that used in [17]. The device shown in Figure 1 is composed of two central steel plates, one with slotted holes and the other with standard clearance holes. Two friction shims of steel coated by thermal sprayed aluminium are sandwiched

on both sides between the central plates and steel cover plate. This whole assembly is fastened together using four preloaded bolts of M12 class 10.9 on the sliding side and six on the fixed side. The design of the linear friction device is carried out according to [26].

The design of the sliding force of the device is calibrated on the instrumentation available at the Laboratory of Materials and Structures of the University of Palermo. Zwick-Roell Z600 universal testing machine, with a maximum load of 600 kN is used. The design is carried out considering, initially, a sliding force equal to 150 kN. Based on the experimental results provided by [8], the friction coefficient for thermal sprayed aluminium is taken as equal to 0.5.

The maximum preload applicable on the bolts is taken as equal to 60% of the preload suggested by the standard (maximum work rate $t_{s,max} = 0.6$). A friction connection is designed using 4 Bolts of M12 class 10.9 bolts having resistant area $A_{res}$ = 85 mm$^2$, yield strength $f_{yb}$ = 900 MPa and tensile strength $f_{ub}$ = 1000 MPa.

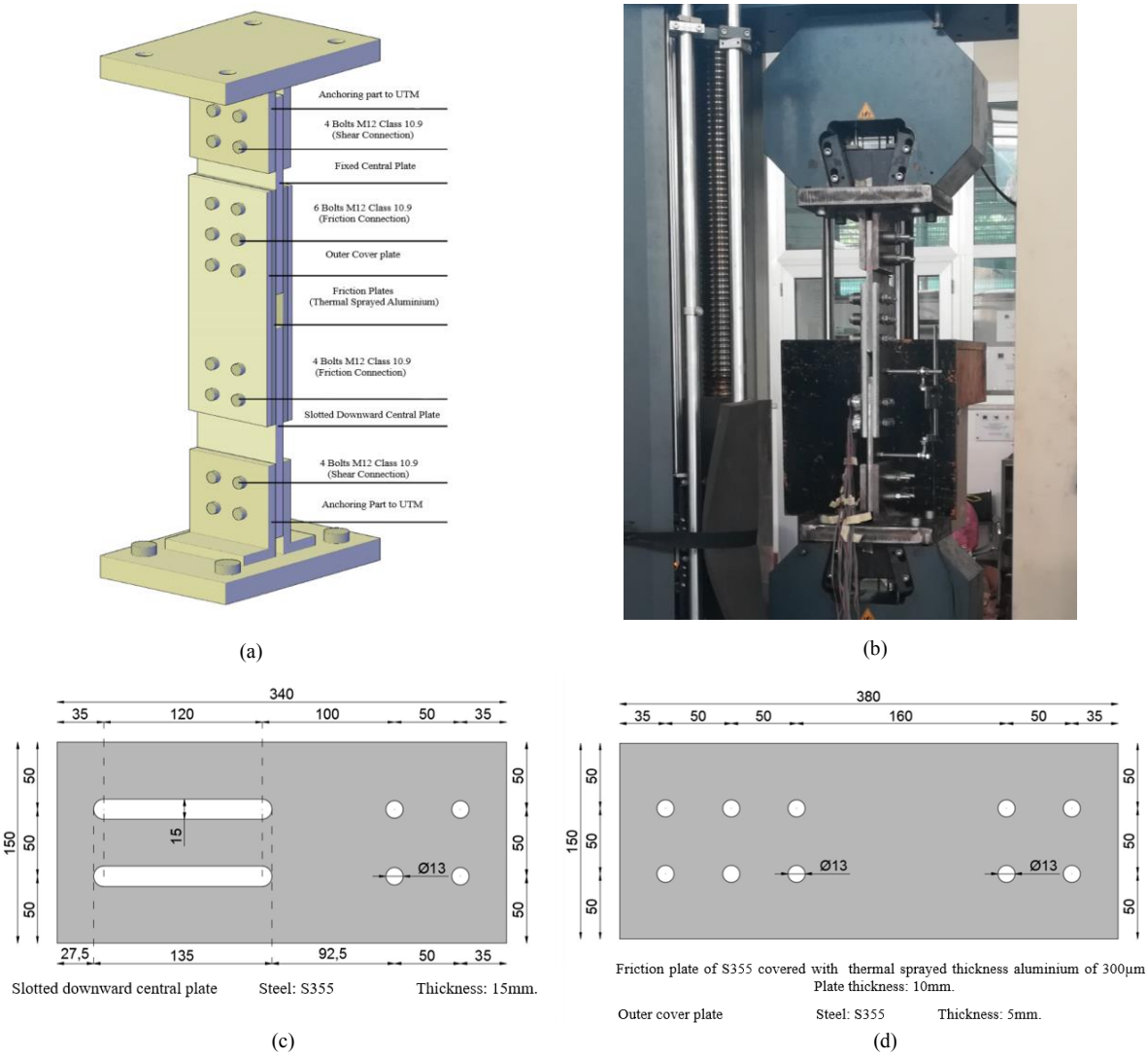


Figure 1: (a) Assembly details of friction dissipative device; (b) friction dissipative device during testing; (c); slotted downward central plate (d) friction plates and outer cover plates

The applicable preload on the bolt according to the regulations is:

$$F_{pc} = 0.7 f_{ub} A_{res} = 59.4 kN \quad (1)$$

Considering two surfaces on which the friction forces of the device are generated ($n_s = 2$), the expected sliding force in the device to be tested is equal to:

$$F_{s,\max} = \mu t_{s,\max} n_s n_b F_{pc} = 0.5 \times 0.6 \times 2 \times 4 \times 59.4 = 142.6 kN \quad (2)$$

## 3 EXPERIMENTAL TESTS ON THE LINEAR FRICTION DISSIPATIVE DEVICE

In the experimental tests, the linear friction device was used to assess the friction properties of the two friction materials (thermal sprayed aluminium and brass). The device was tested using Universal Testing Machine (UTM). The thickness of outer cover plates and friction pads were taken as 10mm and 5mm respectively for all experimental tests. The central plates of the linear friction device were connected using bolted shear connections to four steel angles welded to 35 mm-thick steel plates bolted to the Universal Testing Machine (UTM). The disc springs were used to keep the bolt preload constant on the friction plates as possible. Three-disc springs arranged in series were added to each bolt. The bolt preload was set at 40% of the preload suggested by the standard (maximum work rate $t_{s,\,max} = 0.4$). Thus, the expected experimental sliding force is:

$$F_{s,\max} = \mu t_{s,\max} n_s n_b F_{pc} = 0.5 \times 0.4 \times 2 \times 4 \times 59.4 = 95.04 kN \quad (3)$$

Displacement was monitored by a digital length gauge placed between the fixed downward central plate and the outer cover plate (see Figure 1(b)).

Two tests were carried out for each group of friction shims. Test 1 was performed using new thermal sprayed aluminium plates as friction pads having significant roughness. The force displacement curve of test 1 is shown in Figure 2(a). Two different trends can be seen in the graph, one is where the sliding force is constant and the other is where is a sudden variation of the sliding force. The sudden variation is due to the "stick and slip" phenomenon. It refers to the non-continuous sliding of friction pads and central plate. As it can be seen in Figure 2(a), the plate starts sliding after the attainment of sliding force, and then the force tends to decrease until it stops again and then the load start increasing until the attainment of sliding force. The device

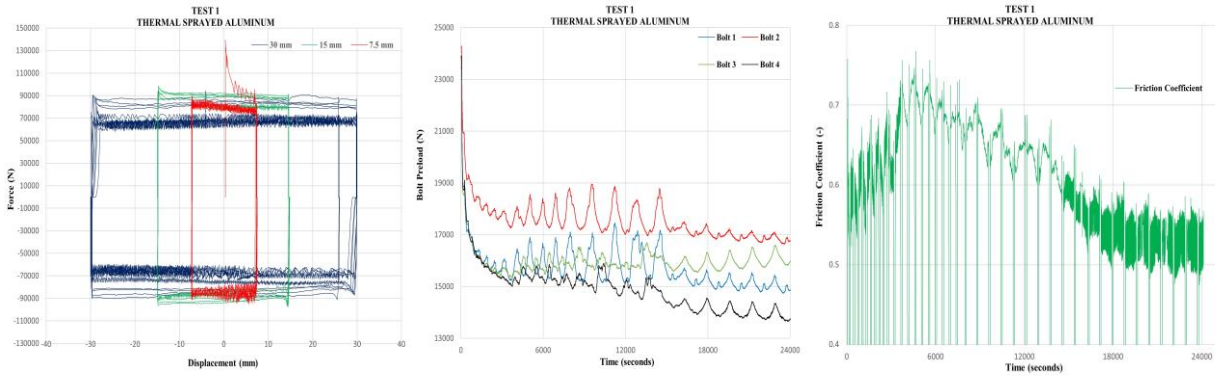


(a) (b) (c)

Figure 2: Results of test 1 for thermal sprayed aluminium (a) force displacement; (b) variation of bolt preload; (c) friction coefficient during test

starts sliding at 140kN and then during the first cycle, the load was significantly reduced up to 90kN. During the last cycles of ± 30mm displacement, the sliding force reduced up to 70kN which is almost half (50%) of the initial sliding force (140kN). Figure 2(b) shows the variation of bolt preload of all four bolts. A decrement in bolt preload can be observed during the test. At the beginning of the test, a large decrement due to the beginning of sliding of the central slotted

plate, namely from 24 kN up to (16 kN-19 kN) occurred, that was not successfully compensated by the disc spring. This phenomenon can be attributed to the sudden reduction of the unevenness of the thermal sprayed aluminium surface produced by a manual treatment. An average of 16 kN bolt load is observed at the end of the test which is almost 33.3% less than the initial bolt preload of 24kN. Figure 2(c) demonstrates the variation of friction coefficient during test 1, evaluated as the ratio of the sliding force and actual instantaneous bolt total load. It can be observed that the friction coefficient increased from 0.62 to 0.75 during the starting phase of the test while at the end of the test, it reduced up to 0.57. Due to this loosening and loss of bolt preload, there is a variation in sliding force and friction coefficient.

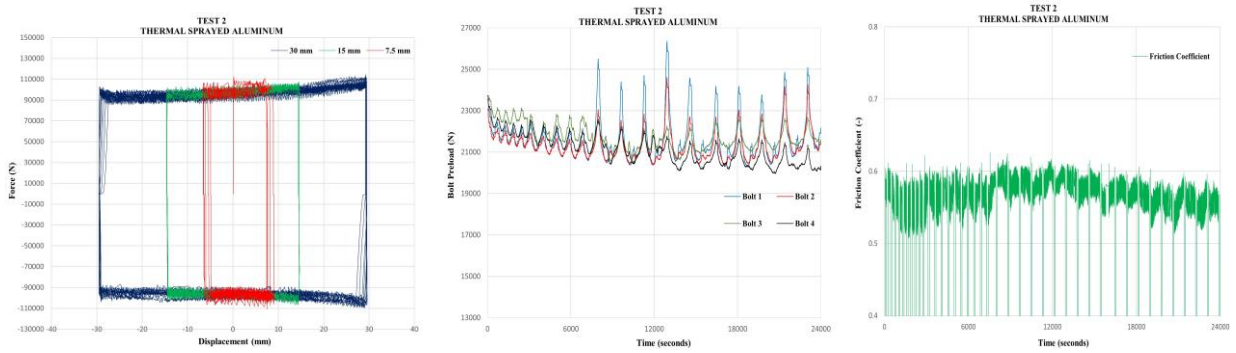


(a) (b) (c)

Figure 3: Results of test 2 for thermal sprayed aluminium (a) force displacement; (b) variation of bolt preload; (c) friction coefficient during test

To get more depth into the phenomenon, and to check the stability of the operational behaviour, test 2 was performed after applying again the bolt preload of 24kN without changing anything in the assembly configuration. The force-displacement curve of test 2 can be seen in Figure 3(a). Unlike the variations as in test 1, there is a very stable curve, and there is not much preload difference between the start and end of the test, proving that the disc spring are able to compensate bolt load fluctuation due to the residual roughness of the sliding surface. The initial sliding force is approximately 110kN while the final sliding force is 94.8kN so the difference is roughly 14% which is much less as compared to the 50% difference observed in test 1.

Similarly, Figure 3(b) shows the trend of bolt preload variation during test 2. It can also be observed that unlike test 1, there is less loss of bolt preload; only 5% loss of bolt preload observed at the start of the test during the initial sliding phase, while the average bolt preload value at the end of the test observed to be 21.5 kN which is 10% less than the initial value, significantly smaller than the loss of bolt preload observed at test 1 (33.3%). The variation of friction coefficient is depicted in Figure 3(c); it can be seen that there is very less variation of friction coefficient at the start phase of test 2 as compared to test 1. The initial friction coefficient is about 0.6 while the final is 0.57.

The results of test 2 are encouraging about the performance of thermal sprayed aluminium. Once the initial unevenness of the surface is reduced by a small number of cycles, the outermost roughness of the surface decreases and the wear rate of thermal sprayed aluminium stabilizes, which provides a stable friction coefficient. Thus, the loss of bolt load and the force-displacement variation is ultimately reduced; as a result, the load-displacement cycles are impressively stable, even for a larger number of cycles than that required by the code [25].

Test 3 was performed using the brass plates as the friction material. The brass seemed to be less rough as compared to thermal sprayed aluminium when touched. Figure 4(a) shows the force-displacement curve; there are large fluctuations in the slip force during the displacement

cycles, and the "stick and slip" phenomenon is more visible in this case. The sliding force increases with the increase of displacement and the number of cycles.
The sliding force was found to be 35kN at the start of the first five cycles of ± 7.5 mm, while it increased up to 62kN at the end of the cycle. At the end of ± 30mm, it was found near about 85kN, which is almost 141% more than the initial sliding value. Variation of bolt preload can be observed in Figure 4(b). Contrary to test 1, there is no loss of bolt preload at the initial phase of the test, and also the average bolt preload remained constant during the whole test. By contrast, in Figure 4(c), it can be seen that the friction coefficient increased as the number of cycles increased, from 0.25 at the start up to 0.42 at the end of the test.

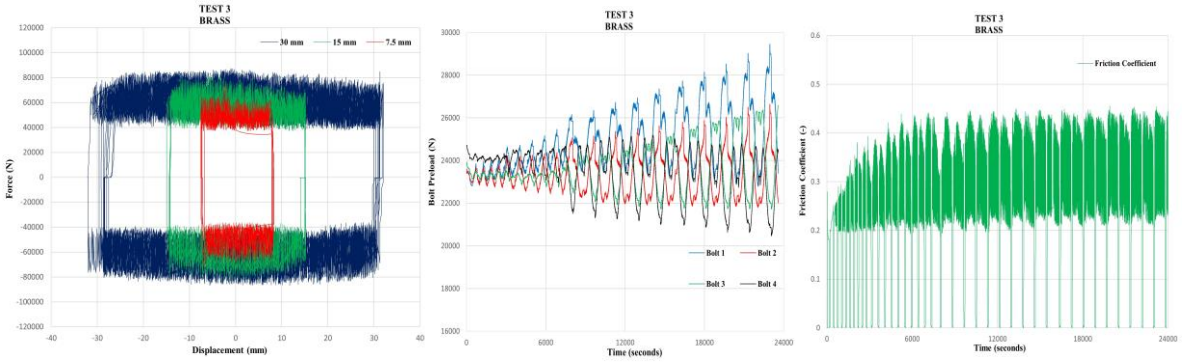


(a) (b) (c)

Figure 4: Results of test 3 for brass (a) force displacement; (b) variation of bolt preload; (c) friction coefficient during test

The increment is due to the wearing out of a brass plate surface, which increased the friction coefficient, and also influenced the force-displacement curve.
To deeply insight into the phenomenon, test 4 was performed after applying again the bolt preload of 24kN on each bolt and without changing the assembly configuration, as done in the previous test 2. Figure 5(a) reports the sliding force-displacement cycles. Unlike test 3, almost constant fluctuation of sliding force is observed for all displacement cycles, with a difference of about 8% from the initial mean to the final mean value, and a very large fluctuation of about 50% of the mean values. The trend of bolt preload as shown in Figure 5(b) demonstrates the high fluctuation during the test, but the average value of bolt preload remained constant at approximately 24kN. The friction coefficient also has large fluctuation, between 0.23 to 0.45, with an almost constant mean value (roughly 0.33) throughout the test as shown in Figure 5(c).

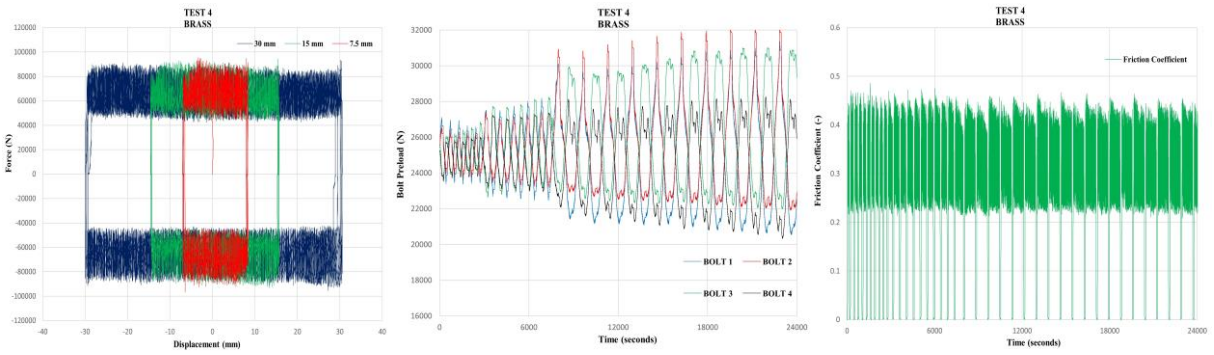


(a) (b) (c)

Figure 5: Results of test 4 for brass (a) force displacement; (b) variation of bolt preload ; (c) friction coefficient during test

By analyzing the results, it can be observed that, unlike thermal sprayed aluminium plates, for the brass plates during cyclic testing, a large fluctuation of the bolt load was obtained in the second test, and consequently a large fluctuation of the friction coefficient was found, both due to the relevant amplitude of the stick and slip phenomenon, that was not adequately compensated by the disc spring. The resulting large fluctuation of the sliding force, even characterized by a constant mean value, proves that the coupling of brass and steel is not as performing as coupling of steel and thermal sprayed aluminium for friction devices.

## 4 FINITE ELEMENT ANALYSIS OF LINEAR FRICTION DISSIPATIVE DEVICE

The Linear friction device was modelled in ABAQUS software as consistent with the experimental specimen shown in Figure 6. In the FEM analysis, to understand the effect of the thickness of friction pads and cover plates on the functioning of the friction device, three different configurations were adopted. In the first configuration, the thickness of thermal sprayed aluminium and outer cover plates were 10 mm and 5mm same as of the experimental specimen. In the second configuration friction shims and outer cove plates were taken thinner 5mm and 2.5mm while for third configuration, taken as thicker of thicknesses 20mm and 10mm respectively as shown in table 1.

| Thickness | Central Plate (mm) | Friction Plate (mm) | Outer Cover Plates (mm) |
|---|---|---|---|
| NT | 15 | 10 | 5 |
| HT | 15 | 5 | 2.5 |
| DT | 15 | 20 | 10 |

*NT=Normal Thickness, HT=Half Thickness, DT=Double Thickness

Table 1: Thickness of plates

To understand the effect of disc springs in maintaining the bolt preload and contact pressure, disc springs were also introduced in the first configuration. They were modelled by a segment of tube, with an internal radius of 13 mm, external radius of 19 mm, height of 12 mm, and elastic modulus able to reproduce the actual disc spring stiffness, that was 14300 N/mm. The bolt preload applied on each bolt was 24 kN, which is equal to 40% of the bolt preload corresponding to the code strength (60 kN), in total a preload of 96 kN was applied on four bolts. On the basis of the experimental results, in FEM modelling the friction coefficient was set equal to $\mu$=0.6. Thus, the expected sliding force is:

$$F_{s,\max} = \mu t_{s,\max} n_s n_b F_{pc} = 0.6 \times 0.4 \times 2 \times 4 \times 59.4 = 114.05 kN \quad (4)$$

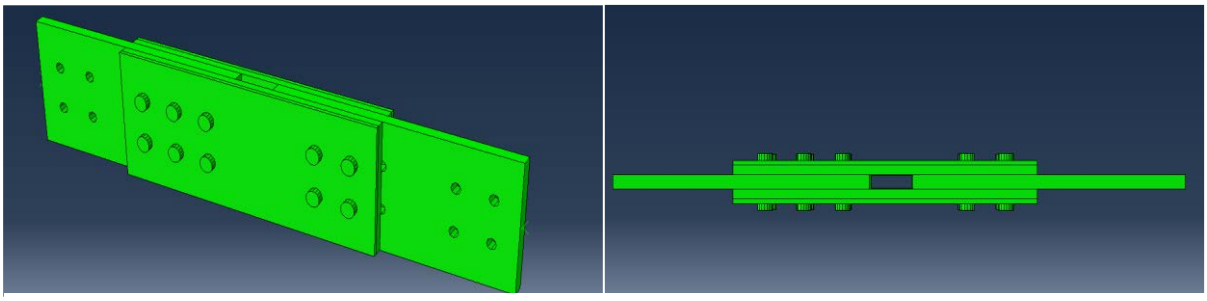

(a) (b)

Figure 6: (3D) views of FEM modelling of linear dissipative device (a) side view; (b) top View

The maximum displacement of the device was assumed as 30mm, consistent with the experimental approach and the loading protocol adopted according to the requirements of [25]. For each analysis, the device was tested by 5 cycles of ± 7.5 mm (25% of maximum displacement), 5 cycles of ± 15 mm (50% of maximum displacement) and 5 cycles of ± 30 mm (100% of maximum displacement).

In Figure 7 the contact pressure distribution of plates in tension (a), (c), (e) and in compression (b), (d), (f) are shown. Figures (a) and (b) represent the results of specimen with double thickness plates, (c) and (d) with normal thickness and (e) and (f) with half thickness.

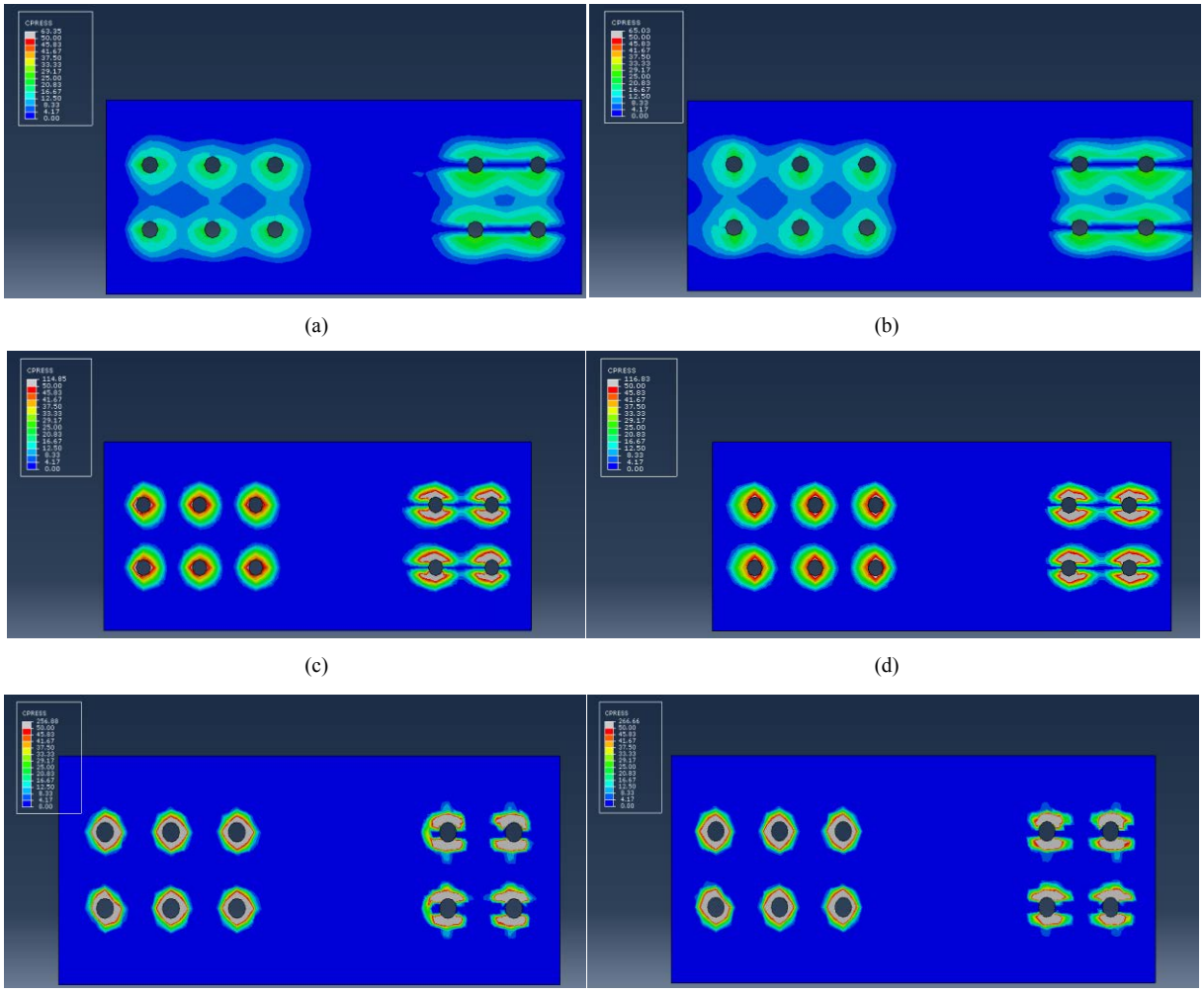

Figure 7: Contact pressure distribution of plates during sliding (a,c,e) in tension; (b,d,f) in compression; (a,b) double thickness; (c,d) normal thickness; and (e,f) half thickness

By comparing Figure 7(a) and Figure 7(b) it can be recognized that in double thick plates the contact pressure is uniformly distributed due to the small deformability of the plates, with a maximum value of 65 Mpa. By contrast, normal thick (Figure 7(c) and Figure(7d)), and half-thick (Figure 7(e) and Figure 7(f)) plates are characterized by stress concentration around the holes. Apparently, the color representation of the contact pressure is very similar, but a deeper inspection of the contact pressure scale focuses that for the latter case, the maximum contact pressure is around 260 Mpa, roughly double as compared to contact pressure for normal thickness plates (115 Mpa). The effect of the different stiffness of the plates of the three specimens on the deformed shape is stressed in Figure 8, where the displacement is magnified by 400%;

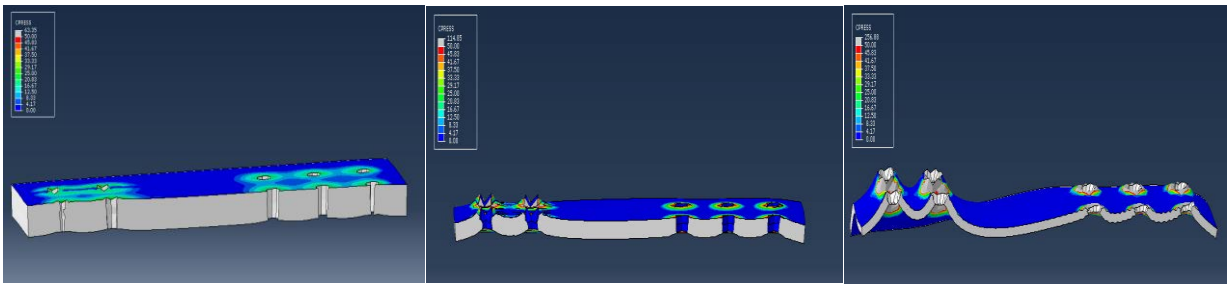

(a) (b) (c)

Figure 8: Deformed shape of plates (a) double thickness; (b) normal thickness; (c) half thickness

the ineffectiveness of the half-thick plate in avoiding transversal deformation can be easily recognized.

In Table 2 the maximum values of the resultant of contact pressure during the sliding phases in compression and tension are reported for the three specimens. A fourth couple of values, related to normal thickness specimen equipped with disc spring (NTWDS), that will be considered in the following, is also reported. The results show that, when sliding in compression is considered, an increment of the resultant of contact pressure, with respect to the initial value of 96 kN, of about 2% for all three specimens is detected; by contrast, when sliding in tension is considered, a reduction is detected, namely 1.6% for DT, 2.8% for NT and 6.45% for HT.

The variation should be attributed mainly to the variation of the plate thickness due to Poisson's effect, and to the uneven distribution of contact pressure especially for half thickness plates. However, it has to be stressed that the FEM model, as it was implemented, was not able to reproduce both the contact pressure variation due to the variation of the unevenness of the sliding surface, nor the variation of the friction coefficient that mainly affects the cycling behaviour of the device.

| Description | Compression (kN) | Tension (kN) |
|---|---|---|
| NT | 98.17 | 93.31 |
| NTWDS | 95.5 | 92.6 |
| HT | 98.22 | 89.8 |
| DT | 97.80 | 94.43 |

NT= Normal Thickness with No Disc Springs, NTWDS= Normal Thickness with Disc Springs
HT = Half Thickness with no Disc Spring, DT = Double Thickness with no Disc Spring

Table 2: Resultant of contact pressure maximum value at tension and compression. Initial value 96 kN.

The FEM model is able to capture the role of the disc spring in reducing the contact pressure variation due to the Poisson effect. To this aim, in Figure 9(a) and Figure 9(b), the distribution of the contact pressure during the sliding phase in tension and compression for the specimen with a normal thickness plate equipped with the disc spring is depicted.

Comparison with Figures 7(c) and 7(d) proves a reduction of the maximum contact pressure in tension of 15.51% and in compression of 22.72%. Regarding the resultant of contact pressure reported in Table 2, it can be recognized that disc springs are able to reduce the fluctuation of the contact pressure during the compression and tension slide phases to 3.4% of the initial value.

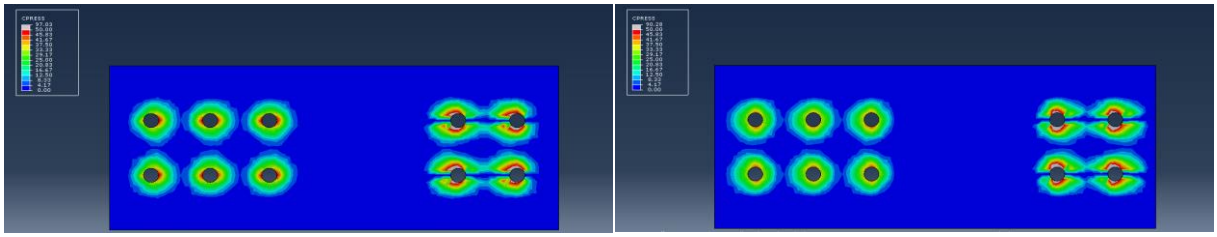

(a) (b)

Figure 9: Contact pressure distribution of plates of normal thickness with disc spring during sliding (a) in tension; (b) in compression.

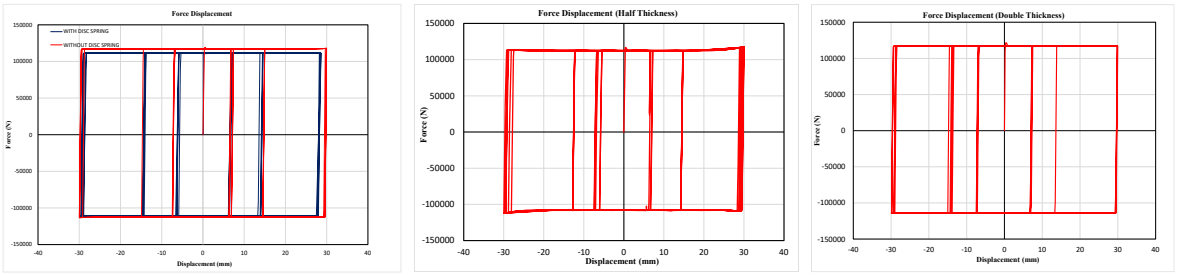


(a) (b) (c)

Figure 10: Force displacement graph for (a) plates of normal thickness with and without disc springs; (b) plates of half thickness; (c) plates of double thickness

The effect of these different configurations on the sliding force-displacement graphs obtained by FEM analysis is shown in Figure 10; the most stable force-displacement relationship behaviour can be observed in plates with normal and double thicknesses, while the force-displacement relationship of half-thickness plates (Figure 10(b)) have some discrepancy for the larger positive and negative displacement, showing that half thickness is not suitable to obtain a stable behaviour. Indeed, a small variation in the sliding force in compression can be observed for the specimen with normal thickness plates, but the presence of disc springs is able to almost eliminate this variation. Table 3 shows the maximum value of the sliding force at the end of

| Description | Compression[kN] | | Tension[kN] | |
|---|---|---|---|---|
| | -30mm | +30mm | -30mm | +30mm |
| NT | 117.13 | 117.83 | 113.13 | 112.23 |
| Difference [%] | 2.70 | 3.31 | -0.81 | -1.60 |
| NTWDS | 111.17 | 111.49 | 112.02 | 112.41 |
| Difference [%] | -2.53 | -2.24 | -1.78 | -1.44 |
| HT | 113.49 | 117.8 | 111.95 | 109.22 |
| Difference [%] | 0.49 | 3.29 | -1.84 | -4.23 |
| DT | 116.51 | 117.04 | 113.74 | 113.92 |
| Difference [%] | 2.16 | 2.62 | -0.27 | -0.11 |

*NT= Normal Thickness with No Disc Springs, NTWDS= Normal Thickness with Disc Springs, HT = Half Thickness with no Disc Spring, DT = Double Thickness with no Disc Spring

Table 3: Maximum value of force displacement graph

± 30 mm last cycle, and the value of the percentage errors with respect to the nominal sliding force (see Equation 4).The values for positive and negative displacement are different due to the different position of the bolts with respect to the slotted downward central plate.

For specimens without disc springs, the difference for positive displacement is mostly larger than the counterpart for negative displacement, and with the exception of HT, the value of the increment in compression is larger than the reduction in tension. The larger differences are found for the half-thick specimen and for positive displacement (-4.23% in tension and +3.29% in compression). The presence of disc springs produces a general reduction of the sliding force, minimizing the fluctuation to 1.09%.

## 5 CONCLUSIONS

Experimental tests on a linear friction dissipative device were performed, and the results were interpreted with the aid of a FEM modelling of the test. The results obtained with thermal sprayed aluminium-steel sliding surfaces were compared with those for brass-steel sliding surfaces. The results prove that the former is able to provide stable and predictable sliding force even for a larger number of cycles than that required by the code [25], once the initial irregularities of the aluminum surface due to manual spraying are reduced through a preventive application of a few load cycles. In this context, a paramount role is played by the role of disc springs when used in conjunction with the thermal sprayed aluminium surface. In friction shims with thermal sprayed aluminium coating, disc springs are able to control the variation of bolt preload that adjusts the sliding force. By contrast, for a brass sliding surface, the stick and slip phenomenon is more pronounced with increased amplitude in the initial cycles which rules the behaviour of the sliding force; this phenomenon is also characterized by undesired large fluctuation during all the subsequent load cycles.

The FEM analysis give more insight into the role of the thickness of the friction and cover plates, proving that the thickness chosen for the tested specimen is the smallest able to ensure a stable value of the sliding force, once is used in conjunction with the disc spring. The FEM analysis showed the disc spring's ability to minimize the variation of the contact pressure due to the Poison effect. Moreover, even if there were small variations of sliding force only, the FEM analysis was able to detect the influence of the relative position of the sliding plates of the device at the end of the cycles in determining the sliding force, and the different behaviour experienced when the sliding plates are loaded in compression and in tension.

## REFERENCES

[1] X.Y. Cao, D. Shen, D.C. Feng, C.L. Wang, Z. Qu, G. Wu, Seismic retrofitting of existing frame buildings through externally attached sub-structures: State of the art review and future perspectives, *Journal of Building Engineering*, **57**,104904, 2022.

[2] M. Ahmed, P. Colajanni, S. Pagnotta. Influence of Cross-Section Shape and FRP Reinforcement Layout on Shear Capacity of Strengthened RC Beams. *Materials*, **15**, 4545, 2022.

[3] S. Benfratello, S. Caddemi, L. Palizzolo, B. Pantò, D. Rapicavoli, S. Vazzano, Targeted steel frames by means of innovative moment resisting connections, *Journal of Constructional Steel Research*, **183**, 106695, 2021.

[4] S. Benfratello, L. Palizzolo, S. Vazzano. A New Design Problem in the Formulation of a Special Moment Resisting Connection Device for Preventing Local Buckling, *Applied Sciences*, **12**, 2022.

[5] T. S. Yang, E. P. Popov, *Experimental and analytical studies of steel connections and energy dissipators, UCB/EERC-95/13,* College of Engineering, University of California, Berkeley, USA, 1995.

[6] H. H. Khoo, G. C. Clifton, J. Butterworth, G. A. MacRae, G. Ferguson, Influence of steel shim hardness on the Sliding Hinge Joint performance, *Journal of Constructional Steel Research*, **72**, 119-29, 2012.

[7] M. Latour, V. Piluso, G. Rizzano, Free from damage beam-to-column joints testing and design of DST connections with friction pads, *Engineering Structures*, **85**, 219-233, 2015.

[8] M. Latour, V. Piluso, G. Rizzano, Experimental analysis of beam-to-column joints equipped with sprayed aluminium friction dampers, *Journal of Constructional Steel Research*, **146**, 33-48, 2018.

[9] S. Ramhormozian, G. C. Clifton, G. A. MacRae, H. H., Khoo, The sliding hinge joint: final steps towards an optimum low damage seismic-resistant steel system, *Key Engineering Materials*, **763**, 751-60, 2018.

[10] P. Colajanni, L. La Mendola, A. Monaco, S. Pagnotta, Dissipative connections of rc frames with prefabricated steel-trussed-concrete beams, *Ingegneria Sismica*, **37**, 51-63, 2020a.

[11] P. Colajanni, L. La Mendola, A. Monaco, S. Pagnotta, Design of RC joints equipped with hybrid trussed beams and friction dampers, *Engineering Structure*s, **227**, 111442, 2021a.

[12] P. Colajanni, S. Pagnotta, Friction-based beam-to-column connection for low-damage RC frames with hybrid trussed beams, *Structural Engineering and Mechanics*, **45(2)**, 231-248, 2022a.

[13] P. Colajanni, L. La Mendola, A. Monaco, S. Pagnotta, Seismic Performance of Earthquake-Resilient RC Frames Made with HSTC Beams and Friction Damper Devices, *Journal of Earthquake Engineering*, **26(15)**, 7787-7813, 2022b.

[14] Y. Cui, Z. Yan, X. Wang, T. Wang, Experimental studies on slip friction device using symmetric friction connections. *Structures,* **44**, 1886-1897, 2022.

[15] A.S. Pall, C. Marsh, Response of friction damped braced frames, *Journal of Structural division, ASCE*, **108**,1313-1322,1982.

[16] Y. Maida, H. Sakata, Finite Element Analysis of Reinforced Concrete Frames with Bracing-Friction Dampers for Seismic Resistance, *Journal of Earthquake Engineering*, 2022.

[17] M. Latour, V. Piluso, G. Rizzano, Experimental analysis on friction materials for supplemental damping devices, *Construction and Building Materials*, **65**, 159-176, 2014.

[18] G.F. Cavallaro, M. Latour, A. B. Francavilla, V. Piluso, G. Rizzano. Standardised friction damper bolt assemblies time-related relaxation and installed tension variability. *Journal of Constructional Steel Research,* **141**,145-55, 2018

[19] G.F. Cavallaro, A. Francavilla, M. Latour, V. Piluso, G. Rizzano, Experimental behaviour of innovative thermal spray coating materials for FREEDAM joints. *Composites Part B: Engineering*, **115**, 289-299, 2017

[20] J.C. Chanchi Golondrino, G.A. MacRae, J.G. Chase, G.W. Rodgers, and G.C. Clifton. Velocity effects on the behaviour of asymmetrical friction connections (AFC). *8th International conference on behavior of steel structures in seismic areas*. Shanghai, China, July 1-3, 2015.

[21] A.F. Santos, A. Santiago, M. Latour, G.Rizzano, L. Simòes da Silva. Response of friction joints under different velocity rates. *Journal of Constructional Steel Research,* **168**, 106004, 2020.

[22] S. Pagnotta, A. Monaco, P. Colajanni, L. La Mendola, Experimental characterization of friction properties of materials for innovative beam-to-column dissipative connection for low-damage RC structures. Giuseppe Ferro, Luciana Restuccia eds, *XIX ANIDIS conference, Seismic Engineering in Italy Procedia Structural Integrity,* Turin, Italy, September 11-15, 2022.

[23] G.A. MacRae, J.G. Chase, G.W. Rodgers, C.G. Clifton, Behaviour of Asymmetrical Friction Connections using different shim materials. *Proceedings of the New Zealand society for earthquake engineering conference.* New Zealand, 2012.

[24] S. Ramhormozian, G. Clifton, S. Maetzig, D. Cvitanich, G. MacRae. Influence of the Asymmetric Friction Connection (AFC) ply configuration, surface condition, and material on the AFC sliding behaviour. In *New Zealand Society for Earthquake Engineering (NZSEE) Annual Technical Conference, Reducing Risk Raising Resilience*. Christchurch, New Zealand, 2016.

[25] CEN EN 15129, anti-seismic devices. CEN, 2018.

[26] EN 1993-1-1, design of joints - Design of steel structures, 2005.